

Super growth of vertically aligned carbon nanotubes on pulsed laser deposited catalytic thin films

D. Fejes · Z. Pápa · E. Kecsenovity ·
B. Réti · Z. Toth · K. Hernadi

Received: 15 October 2014 / Accepted: 21 December 2014 / Published online: 18 January 2015
© Springer-Verlag Berlin Heidelberg 2015

Abstract Efficient and reproducible growth of vertically aligned carbon nanotube (CNT) forests by catalytic chemical vapor deposition (CVD) requires precise setting of the properties of the catalyst thin films and CVD conditions. In this work, super growth of vertically aligned CNTs onto Al_2O_3 support and Fe–Co catalyst layer system is presented. The layers were grown by pulsed laser deposition (PLD) onto silicon wafer pieces. Their thickness and optical properties were controlled by spectroscopic ellipsometry. The effect of heat treatment at 750 °C in nitrogen and in hydrogen of these PLD layers was compared. High-resolution electron microscopic images showed that treatment of catalyst layers in H_2 resulted in finer and denser catalytic particles. As a result, well-aligned, dense and few-walled CNT forests with 1–1.5 mm height were deposited by water-vapor-assisted CVD on the hydrogen-treated films, while without hydrogen treatment defected CNT structures were grown. According to these observations, Raman spectroscopy showed a higher degree of crystallinity in case of CNT-s, where reduction by hydrogen influenced the oxidation state of the metallic catalytic particles in a beneficial way.

1 Introduction

Since the first synthesis in 1996 [1], vertically aligned carbon nanotubes (CNTs) have become a focus of research in nanoscience and nanoengineering. The most efficient way to produce vertically aligned CNTs is catalytic chemical vapor deposition (CVD). A transition metal, such as Fe, Co, Ni or their alloys, is commonly used as catalyst, while Al_2O_3 , MgO and SiO_2 are the best oxide supports [2–6]. In 2004, Hata et al. [7] developed the enhanced carbon nanotube CVD growth by introducing traces of water together with the carbon source. CVD parameters of efficient CNT growth are well established. However, the properties of the support catalytic layer system sensitively influence the final result, i.e., density, orientation, length, thickness and crystalline quality of the CNTs.

The most important properties of the catalytic layer are the thickness, composition, density and adherence, which have a significant role during the catalytic synthesis. Magnetron sputtering [8, 9], radio frequency sputtering [10, 11], electron beam evaporation [12–14] and physical vapor deposition [15] were typically used to produce catalyst layers.

Pulsed laser deposition (PLD) is an extremely versatile technique for preparing a wide range of thin films and multilayer structures, in superior quality. PLD has a very simple experimental setup, and it consists of targets, a substrate and their holders housed in a vacuum chamber. A high-power pulsed laser is used as an external energy source to vaporize target materials and to deposit thin films in congruent way which means stoichiometric material transfer between the target and the substrate. Due to the energetic plasma, the laser deposited films are dense and adhere well on the substrate. In contrast to the simplicity of the setup, the theoretical descriptions of laser–target

D. Fejes · E. Kecsenovity · B. Réti · K. Hernadi (✉)
Department of Applied and Environmental Chemistry,
University of Szeged, Rerrich B. ter 1., Szeged 6720, Hungary
e-mail: hernadi@chem.u-szeged.hu

Z. Pápa · Z. Toth
Department of Optics and Quantum Electronics, University of
Szeged, Dom ter 9., Szeged 6720, Hungary

Z. Toth
Department of Oral Biology and Experimental Dental Research,
University of Szeged, Tisza Lajos krt. 64., Szeged 6720,
Hungary

interaction are very complex [16–18]. The mechanism that leads to material ablation depends on laser characteristics, as well as the optical, topological and thermodynamical properties of the target [17, 18]. Thickness of the deposited layer can be controlled precisely even in atomic scale, since there is a linear connection between the number of laser pulses and the layer thickness.

The aim of this work was to investigate pulsed laser deposited layer system as a catalyst support for carbon nanotube growth. The ability to deposit different kinds of materials in a pre-defined composition, and sensitive thickness control were the main advantages why PLD was chosen as a preparation tool for the catalyst layer system. Initial results were reported by a few groups to grow CNTs on catalyst layers produced by PLD [19–21]. However, the length of the resulted nanotube carpets was moderate. In our approach, the thickness control of the support and the catalyst layer was done by *ex situ* spectroscopic ellipsometry (SE). It is an effective, nondestructive optical method, which can check layer thicknesses and quality after each deposition process. Performing ellipsometric measurement on test samples after each deposition step enabled us to calibrate deposition rates and prepare the layer system with sub-nanometer accuracy.

2 Experimental

Catalyst layers were prepared by PLD. Laser pulses from an ArF excimer laser (LLG TWINAMP, wavelength 193 nm, pulse length 18 ns, repetition rate 10 Hz) were focused onto a pressed Al₂O₃ target. The average fluence was 13 J/cm². The pulse energy variation during an experiment was ~10 %. The target was rotated to prevent the formation of deep ablation grooves. A *p*-type (100) silicon substrate with thickness of 0.8 mm was placed at a distance of 3 cm from the target. Al₂O₃ layers were deposited in 1 Pa oxygen background. Afterward, the target was changed to a pressed Fe–Co target (2:1 molar ratio). Fe–Co layers were deposited onto the Al₂O₃-coated silicon in vacuum ($p < 5 \cdot 10^{-2}$ Pa). Test samples with thick layers were produced firstly. Ellipsometric measurements after the deposition steps were performed with a rotating compensator spectroscopic ellipsometer (Woollam M-2000F) in the 275–1,000 nm (1.24–4.5 eV) range. Film thicknesses, refractive index values and absorption coefficients were determined on these test samples by SE. Based on these results, the appropriate pulse numbers were determined to deposit layers that were used for CNT growth. The structure of these samples was also checked by SE.

To perform CVD synthesis, PLD catalyst layers were placed into a fixed-bed flow quartz tube reactor (diameter is

20 mm, length 800 mm) at 750 °C. The reaction time was 30 min, preceded by a 5-min nitrogen purge. Half of the samples were treated by an additional 5-min reduction with hydrogen (gas flows: 100 and 80 mL/min, respectively). To start the growth of CNTs, ethylene (100 mL/min) was introduced to the system. At the beginning of the synthesis, at the same time as ethylene was launched, 25 mL/min nitrogen gas flow was bubbled through 25 °C water for enhancing the carbon nanotube growth [7]. After 30 min, the system was cooled down.

Orientation of the CNTs was recorded by a Hitachi S-4700 field emission cathode scanning electron microscope (FESEM) in secondary electron imaging mode. Transmission electron microscope (TEM) micrographs were imaged by FEI Tecnai G² 20X-Twin-type transmission electron microscope. Raman spectra of the samples were recorded using a Thermo DXR Raman microscope in the 50–1,860 cm⁻¹ range with ~3 cm⁻¹ resolution. The excitation wavelength was 532 nm. The spectra were taken by 5 mW laser power, which was focused onto the nanotubes by a 50× magnification microscope objective for 2·10 s.

3 Results

3.1 Preparation of catalyst layers

As an initiator of the CNT growth, the quality of the support and the catalyst layer has a determining role. In the followings, the most important properties of the catalyst will be presented in detail from the perspective of PLD. Film thicknesses of the catalyst layers were chosen based on previous CNT CVD experiments [22–24].

For Al₂O₃ test layers, a series of experiments were performed with different pulse numbers. For evaluation of SE measurements, a simple Cauchy model was applied, since with this simple polynomial fit, refractive index dispersion for transparent materials can be described. The structure of the ellipsometry model was the following: silicon substrate–native silicon dioxide–Al₂O₃. The Fe–Co layers were deposited onto the Al₂O₃ layers. The structure of the ellipsometry model was extended as follows: silicon substrate–native silicon dioxide–Al₂O₃–Fe–Co alloy layer. To describe Fe–Co alloy layer, a general oscillator layer [25] was applied: the combination of two Gaussian oscillators allowed a sufficient description of the absorption properties, i.e., the imaginary part of the dielectric function.

The density of the PLD films correlates with the refractive index of the films, since refractive index is proportional to the atomic density of the material. The bulk and the thin film refractive indices are presented in

Table 1 Bulk and thin film refractive indices of the deposited materials

	Bulk refractive index @ 532 nm	Layer refractive index @ 532 nm
Fe	2.8954 [26]	2.2015 ± 0.2887
Co	2.0014 [26]	
Al ₂ O ₃	1.7728 [27]	1.5740 ± 0.0252

Table 1. These results show that layer densities are slightly smaller than the bulk material density in case of Al₂O₃, which can be considered as very dense one among thin films. However, the refractive index of the catalyst layer is lower than the bulk iron and slightly higher than cobalt. Dispersion of optical properties of the Fe–Co layers is appropriate for proving their metallic character.

Layer thickness can be controlled precisely by PLD and measured by SE. In Fig. 1, the thickness values of the test Al₂O₃ layers are plotted as a function of pulse number. The slope of the linear fit gives the deposition rate, which is 0.00282 nm/pulse. This thickness is much lower than the thickness of one atomic layer. Choosing the appropriate pulse number, thickness could be controlled on an atomic scale. However, the laser plume inhomogeneity and the energy fluctuation of the laser pulses result in $\sim 10^{-4}$ nm/pulse error in the thickness, which is determined from the accuracy of the linear fit shown in Fig. 1.

Test layers of Fe–Co alloy were deposited with 600, 1,000 and 12,000 laser pulses. The average deposition rate was 0.00839 nm/pulse.

Based on the experiences of test sample depositions, Al₂O₃ and Fe–Co layers were produced with 3,000 and 600 laser shots, respectively. The SE analysis proved that the obtained layer thicknesses were close to the desired ones, which are 10 and 4.5 nm, respectively. Standard deviation in the thickness values of both the Al₂O₃ and Fe–Co layer is around 0.6 nm in a 1×1 cm² area. While infrared absorption can be observed in a case of thicker (>100 nm) test layer, the thin catalyst layer did not show this feature, which can be a sign of partial oxidation.

3.2 Catalyst particle formation and CNT growth

Results in the literature show that the oxidation state of the catalyst particles significantly affects the length and diameter of the synthesized nanotubes [14, 28]. It was also found [22, 28] that a reductive environment created by the hydrocarbons is not enough to reduce the metal in the catalyst particles and hydrogen pretreatment is also necessary. A lot of papers can be found on the direct effect of hydrogen onto the enhanced growth of CNTs, but the intermediate phase of the catalyst wafer is less

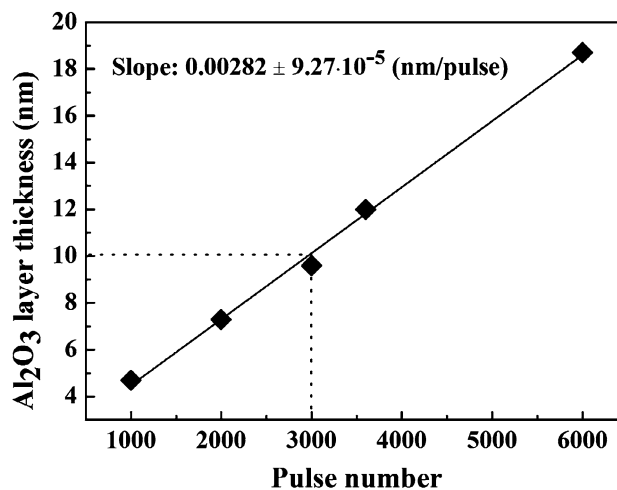


Fig. 1 Thickness values of the test Al₂O₃ layers as a function of pulse number. Slope of the fitted curve provides the deposition rate. Dotted lines show the desired thickness value for catalyst support and the relating pulse number

studied. Mata et al. investigated the substrate annealing conditions by comparing three in situ treatment approaches (Ar, Ar/H₂ mixture and their combination). They concluded that heating in Ar only no particles were formed. In the cases of the application of combined Ar/H₂ treatments, particles were formed with the same size. The ones obtained only for Ar/H₂ mixture have slightly lower density, indicating that the Fe film did not fully converted into particles [29]. We investigated the effects of preliminary reduction process on the thin film catalyst. In Fig. 2a, SEM image from an as-prepared catalyst layer surface is presented. The smooth surface of the PLD layer is in contrast to the surface of annealed samples in nitrogen and hydrogen (Fig. 2b, c). High temperature resulted in droplet formation of the top layer. The size distribution and the number of the droplets are strongly affected by reduction in hydrogen.

Particle size distributions were calculated using the SEM images presented above. Evolving particles on the samples in case of heat treatment and when both heat treatment and reduction were performed are presented in Fig. 3. As can be seen, reduction resulted in smaller particle radii and the presence of larger amount of catalyst centers (c.f. Fig. 2b, c). The mobility of the oxidized metal particles is restricted at the Al₂O₃–catalyst interface [29]. The reduction leads to less-oxidized layer with different wetting properties and enhanced particle mobility. The formation of relatively smaller particles compared with the case of N₂ treatment can be caused by the loss of oxygen in the metal oxide particles. It is known that smaller catalyst particles are favorable for small diameter, few-walled nanotube growth.

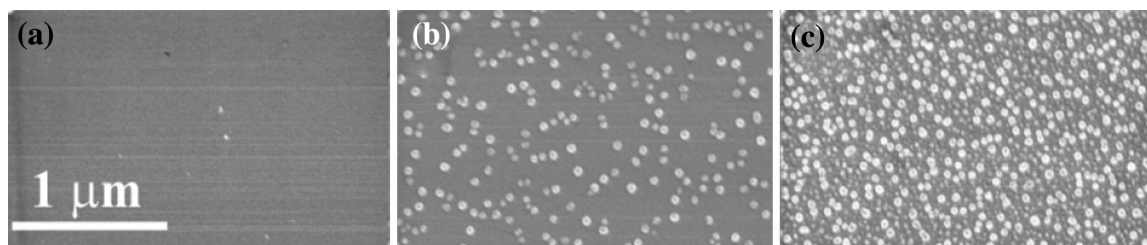


Fig. 2 SEM images from **a** the surface of the intact PLD layer system, **b** after 750 °C heat treatment in N₂ and **c** after heat treatment with reduction in H₂. High temperature resulted in droplet formation on the top layer

Fig. 3 **a** Particle size distribution in case of heat treatment and **b** the distribution when both heat treatment and reduction were performed. Smaller droplets dominate when H₂ gas flow was applied

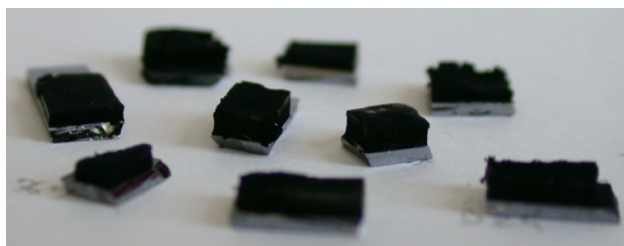
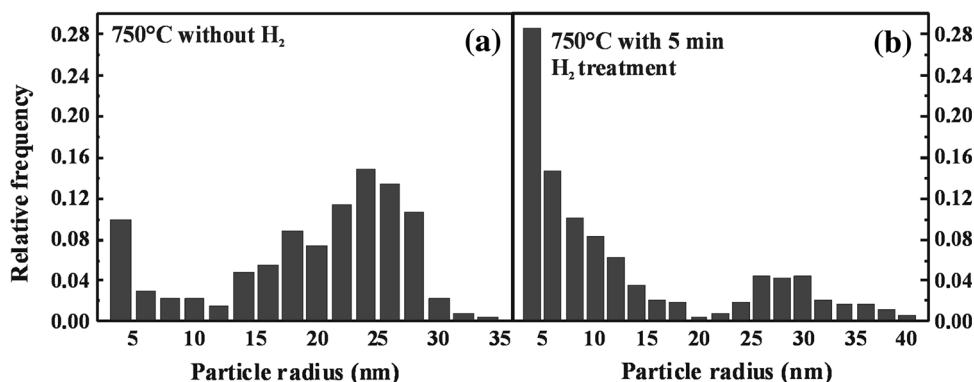


Fig. 4 Image of typical CNT forests. Note that the thickness of the Si wafer pieces is 0.8 mm

For CNT growth, traces of water were added to the gas mixture, i.e., water-assisted CVD was performed. The presence of water is known to enhance the CVD process by etching the co-deposited amorphous carbon and to improve the dehydrogenation and aromatization rate of the hydrocarbon source [22].

The PLD layers resulted in high catalytic activity and CNT forests were produced during the CVD process in case of H₂ pretreatment. The image of typical CNT forests can be seen in Fig. 4. Well-aligned, dense CNT forests have been grown on the pulsed laser deposited catalyst layers. In Fig. 5, the height distribution of the synthesized nanotube forests is shown. The average height of the nanotubes is around 1 mm. Highest CNT forests reached even the height value of 1.5 mm. As a result of high-quality catalyst layer system and optimized CVD growth

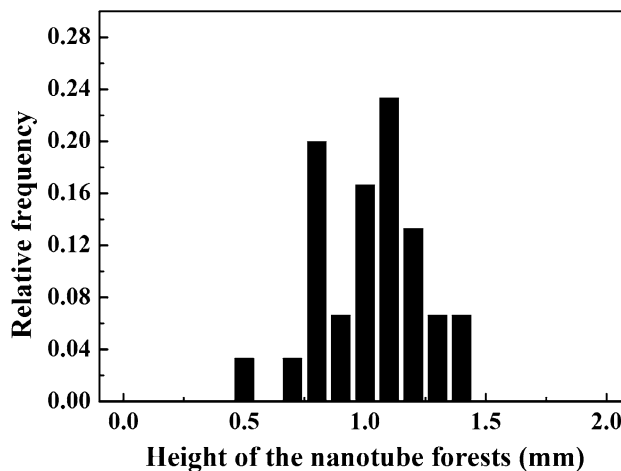


Fig. 5 Height distribution of the synthesized nanotube forests in case of H₂ pretreatment of the catalyst layer

parameters, high growth rates could be reached in the 2–3 mm/h range during our deposition period.

Without the preliminary reduction process of the catalyst wafer, the average height of the nanotube forest was only maximum 150 μm.

SEM micrographs of the forests show that CNTs grown by applying H₂ are longer and better aligned (Fig. 6b, d, f) than in the other case, grown without H₂ (Fig. 6a, c, e). TEM images reveal that CNTs with high quality and clean surface were produced using H₂ treatment (Fig. 6h). Based

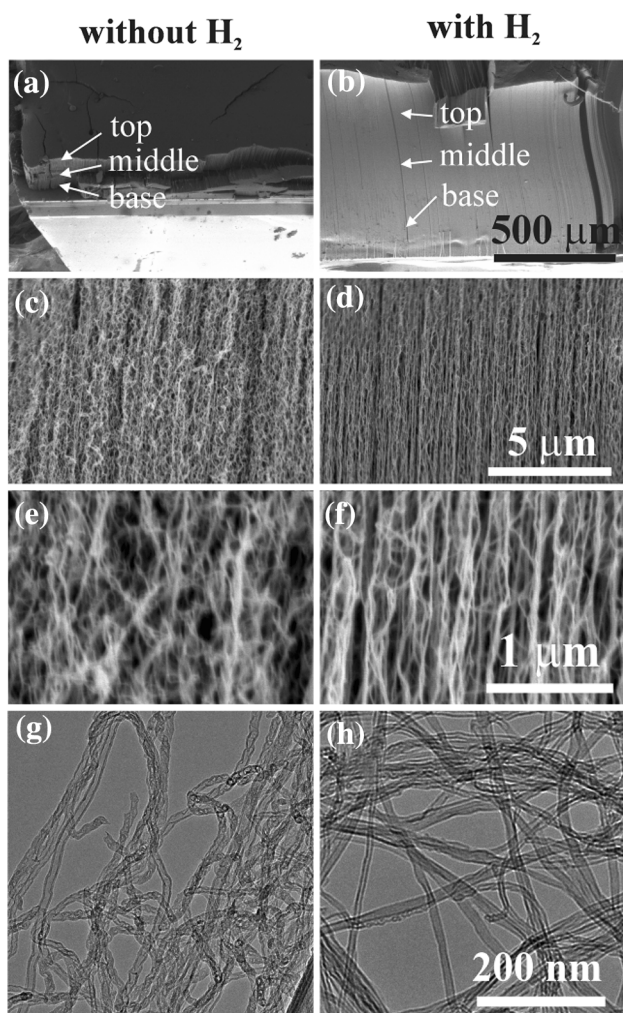


Fig. 6 Both types of as-prepared carbon nanotube forests were investigated and characterized by SEM and TEM. Figure 6a, c, e and g micrographs on the left side of the picture correspond to the carbon nanotube forest synthesized without H_2 . Figure 6b, d, f, h representative images of a carbon nanotube forest grown using H_2 . Note that SEM images were taken by tilting the samples at 45° . Therefore, the apparent height is smaller than the actual height of the forests

on our observations, the nanotubes have 2–5 walls, so they belong to the group of few-walled CNTs. The outer diameter distribution indicates that nanotubes with 11 nm diameters are dominating in the forest synthesized without hydrogen, while the forests produced by applying hydrogen are mainly dominated by nanotubes with diameters of 9–14 nm (Fig. 7). The wider distribution obtained in the case of H_2 -treated samples correlates with the wider distribution of the nanoparticle radii (c.f. Fig. 3).

The two kinds of CNT carpets have been analyzed by micro-Raman spectroscopy at different positions (c. f. Fig. 6a, b). In order to gain information about different parts of the sample, individual spectra were taken at the base, at the middle and at the top of the carpets. Spectra

were analyzed and intensity ratio of D and G bands was calculated to get insight of the structure of the CNTs. High I_D/I_G ratio indicates disordered structure and more defects; thus, lower ratio means better, more defined graphitic structure with fewer defects [30, 31]. Figure 8a shows two examples from the measured Raman spectra, and in Fig. 8b, the calculated I_D/I_G ratios at different positions of CNT carpets are plotted. Both samples, synthesized with H_2 and without H_2 pretreatment, show increasing I_D/I_G ratio from the top to the base, which means decrease in CNT quality during the CVD growth. Water injection for the last 5 min of the synthesis process was stopped, so at the final part of the growth (which occurs at the base) it could not benefit from the effect of water. Moreover, the top parts of the samples were exposed longer to high temperature and water vapor than the base, so more graphitized structure could form there. Thus, this can explain higher I_D/I_G at the base. The two samples show difference in I_D/I_G ratios at each measurement points. H_2 -treated sample has much lower I_D/I_G ratio compared with the one prepared without it.

Prior to the synthesis process, the H_2 reduces the catalyst layer at higher extent than ethylene, thus providing new surface properties of the Fe–Co alloy layer. A cleaner metallic surface influences the melting point and surface tension of the thin film at nanoscale, and smaller metal catalyst particles can form with increased catalyst activity. This leads to straighter, better-quality CNTs formation, while without H_2 the partially reduced metal catalyst particles promote the formation of curlier, more defected CNTs.

In summary, both the quality of the catalyst layer system and the optimized CVD circumstances contributed to the efficient CNT synthesis. There are several opportunities for further optimization, e.g., to find appropriate Fe–Co thickness, composition, layer densities and structures of catalyst layers. Already these nanotube forests can be applied, e.g., to produce yarns, sheets and nanocomposites with oriented CNT fillers. The narrow diameter distribution and uniform CNT length makes these few-walled CNT forests appropriate for, e.g., microelectronic, electrochemical, sensor and biological basic and applied research.

4 Conclusions

In this work, a method is presented where PLD and catalytic CVD are combined in order to grow carbon nanotube forests. Both PLD and CVD are widely available, simple and cost-effective techniques, and the resulting nanotube forests have high quality: The height of the forests can reach even the value of 1.5 mm consisted of well-aligned, few-walled CNTs. The thickness and the quality of the

Fig. 7 **a** Distribution of the outer diameter of CNTs based on TEM investigations in case of heat treatment and **b** the distribution when both heat treatment and reduction were performed

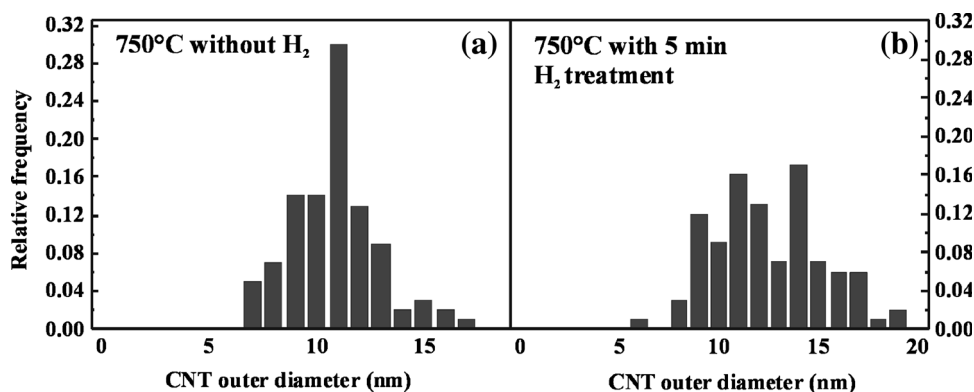
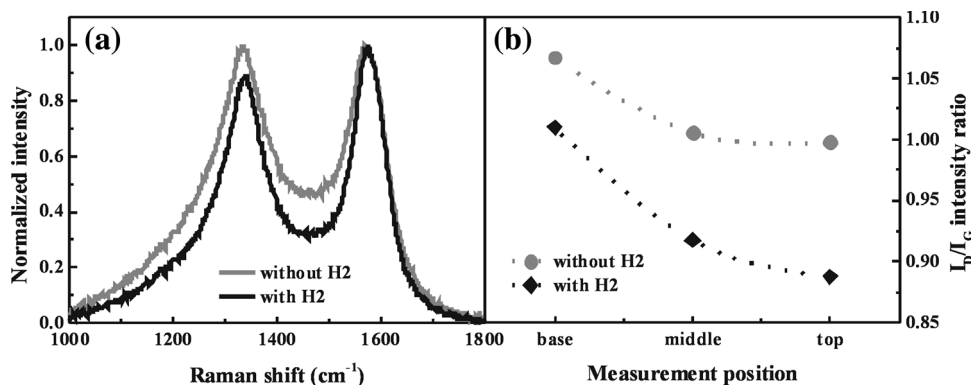


Fig. 8 **a** Typical Raman spectra of the top positions of the nanotubes grown on hydrogen-treated and non-treated catalyst layers. **b** I_D/I_G ratios calculated from Raman spectra recorded at different positions of the two kinds of nanotube forests. Circles and squares show the results of the forests synthesized without and with H_2 pretreatment, respectively



PLD layers can be controlled precisely by combining deposition with ellipsometric measurements. The effect of the catalyst reduction was also investigated. We have proved the role of hydrogen pretreatment before CVD. It turned out that in these experiments the H_2 treatment of the catalyst is necessary for enhancing the formation of catalytic particles and influences their oxidation state in a beneficial way, therefore increasing their lifetime and efficiency. As a result, on hydrogen-reduced catalyst layer system, higher nanotube forests were obtained with increased graphitization and uniform alignment. Further investigations are in progress in order to clarify the role of layer thicknesses, compositions and structure using the flexibility of PLD method.

Acknowledgments This work was supported by Grants from Switzerland through the Swiss Contribution (SH/7/2/20). The work of Z. Pápa was supported by the European Union and the State of Hungary, co-financed by the European Social Fund in the framework of TÁMOP 4.2.4. A/2-11-1-2012-0001 'National Excellence Program'.

References

1. W.Z. Li, S.S. Xie, L.X. Qian, B.H. Chang, B.S. Zou, W.Y. Zou, R.A. Zhao, G. Wang, *Science* **274**, 1701 (1996)

2. S. Noda, K. Hasegawa, H. Sugime, K. Kakehi, Z.Y. Zhang, S. Maruyama, Y. Yamaguchi, *Jpn. J. Appl. Phys.* **46**, L399 (2007)
3. C. Mattevi, C.T. Wirth, S. Hofmann, R. Blume, M. Cantoro, C. Ducati, C. Cepek, A. Knop-Gericke, S. Milne, C. Castellarin-Cudia, S. Dolafi, A. Goldoni, R. Schloegl, J. Robertson, *J. Phys. Chem. C* **112**, 12207 (2008)
4. S. Sakurai, H. Nishino, D.N. Futaba, S. Yasuda, T. Yamada, A. Maigne, Y. Matsuo, E. Nakamura, M. Yumura, K. Hata, *J. Am. Chem. Soc.* **134**, 2148 (2012)
5. J. Robertson, G.F. Zhong, C.S. Esconjauregui, B.C. Bayer, C. Zhang, M. Fouquet, S. Hofmann, Applications of carbon nanotubes grown by chemical vapor deposition. *Jpn. J. Appl. Phys.* **51**(1), 01AH01 (2012)
6. N. Halonen, K. Kordas, G. Toth, T. Mustonen, J. Maklin, J. Vahakangas, P.M. Ajayan, R. Vajtai, *J. Phys. Chem. C* **112**, 6723 (2008)
7. K. Hata, D.N. Futaba, K. Mizuno, T. Namai, M. Yumura, S. Iijima, *Science* **306**, 1362 (2004)
8. T. Arcos, P. Oelhafen, D. Mathys, *J. Phys. Chem B* **108**, 7728 (2004)
9. D.P. Burt, M.W. Whyte, J.M.R. Weaver, A. Glidle, J.P. Edgeworth, J.V. Macpherson, P.S. Dobson, *J. Phys. Chem. C* **113**, 15133 (2009)
10. R.G. Lacerda, K.B.K. Teo, A.S. Teh, M.H. Yang, S.H. Dalal, D.A. Jefferson, J.H. Durrell, N.L. Rupesinghe, D. Roy, G.A.J. Amaratunga, W.I. Milne, F. Wyczisk, P. Legagneux, M. Chhowalla, *J. Appl. Phys.* **96**, 4456 (2004)
11. Z.F. Ren, Z.P. Huang, J.W. Xu, J.H. Wang, P. Bush, M.P. Siegal, P.N. Provencio, *Science* **282**, 1105 (1998)
12. Y. Yao, L.K.L. Falk, R.E. Morjan, O.A. Nerushev, E.E.B. Campbell, *J. Mat. Sci. Mat. Electron.* **15**, 533 (2004)

13. G. Eres, A.A. Puzos, D.B. Geohegan, H. Cui, *Appl. Phys. Lett.* **84**, 1759 (2004)
14. E. Teblum, Y. Gofer, C.L. Pint, G.D. Nessim, *J. Phys. Chem. C* **116**, 24522 (2012)
15. M. Dubosc, S. Casimirius, M.-P. Besland, C. Cardinaud, A. Granier, J.-L. Duvail, A. Gohier, T. Minea, V. Arnal, *J. Microelectron. Eng.* **84**, 2501 (2007)
16. D. Bäuerle, *Laser Processing and Chemistry*, 4th edn. (Springer, Berlin, 2011), pp. 489–531
17. D.B. Chrisey, G.K. Hubler (eds.): *Pulsed Laser Deposition of Thin Films*. Wiley, New York, (1994) p. 23, p. 89
18. H.U. Krebs, in *Pulsed Laser Deposition of Thin Films*, ed. by R. Eason (Wiley, New York, 2007), pp. 363–380
19. S. Neralla, S. Yarmolenko, J. Sankar, J.V. Shanov, Y.H. Yun and M.J. Schulz, *Mater. Res. Soc. (Symposium Proceedings)*, 900, 433 (2005)
20. M. Gaillard, E. Amin-Chalhoub, C. Boulmer-Leborgne, A. Petit, E. Millon, N. Semmar, *AIP Conf. Proc.* **1464**, 179 (2012)
21. T. Ižák, M. Veselý, T. Daniš, M. Marton, M. Michalka, M. Kadlečíková, *J. Phys. Conf. Ser.* **100**(1), 072008 (2008)
22. A. Magrez, R. Smajda, J.W. Seo, E. Horvath, P.R. Ribič, J.C. Andresen, D. Acquaviva, A. Olariu, G. Laurency, L. Forró, *ACS Nano* **5**, 3428 (2011)
23. R. Smajda, J.C. Andresen, M. Duchamp, R. Meunier, S. Casimirius, K. Hernádi, L. Forró, A. Magrez, *Phys. Status Solidi B* **246**, 2457 (2009)
24. A. Magrez, J.W. Seo, R. Smajda, M. Mionic, L. Forró, *Materials* **3**, 4871 (2010)
25. D. De Sousa Meneses, M. Malki, P. Echegut, *J. Non-Cryst. Solids* **352**, 769 (2006)
26. P.B. Johnson, R.W. Christy, *Phys. Rev. B* **9**, 5056 (1974)
27. T. Lichtenstein, *Handbook of Thin Film Materials* (College of Engineering and Applied Science, University of Rochester, Rochester, 1979)
28. J. Dijon, P.D. Szkutnik, A. Fournier, T. Goislard de Monsabert, H. Okuno, E. Quesnel, V. Muffato, E. De Vito, N. Bendiab, A. Bogner, N. Bernier, *Carbon* **48**, 3953 (2010)
29. D. Mata, R.M. Silva, A.J.S. Fernandes, F.J. Oliveira, P.M.F.J. Costa, R.F. Silva, *Carbon* **50**, 3585–3606 (2012)
30. M.S. Dresselhaus, G. Dresselhaus, R. Saito, A. Jorio, *Phys. Rep.* **409**, 47 (2005)
31. E.F. Antunes, A.O. Lobo, E.J. Corat, V.J. Trava-Airoldi, A.A. Martin, C. Verissimo, *Carbon* **44**, 2202 (2006)